ISSN 2723-6471

Combined Fire Fly – Support Vector Machine Digital Radiography Classification (FF-SVM-DRC) Model for Inferior Alveolar Nerve Injury (IANI) Identification

P. Manikandaprabhu[1,*], C. Thirumoorthi[2], M. Batumalay[3], Zhengrui Xu[4]

[1]*Department of Computer Science, School of Computing, Amrita Vishwa Vidyapeetham, Mysuru, Karnataka, India*

[2]*Department of Computer Science, PSG College of Arts and Science, Coimbatore - 641 014, India*

[3]*Faculty of Data Science and Information Technology, INTI International University, 71800 Nilai, Negeri Sembilan, Malaysia*

[4]*Faculty of Liberal Arts, Shinawatra University (SIU) Pathum Thani 12160 Thailand*

(Received: June 21, 2024; Revised: July 14, 2024; Accepted: August 28, 2024; Available online: September 17, 2024)

Abstract

Inferior Alveolar Nerve Injury (IANI) is a severe complication in oral surgery that can significantly affect a patient's quality of life. Accurate diagnosis is crucial for effective management, and digital radiography has become an essential tool in this regard. This study proposes a novel feature selection-based classification algorithm to enhance the diagnostic precision of digital radiographs (DRs) for IANI detection. The objective is to improve classification accuracy by selecting the most relevant features using a Firefly algorithm-based method. Our approach identifies optimal features that preserve critical information from the dataset, enabling more accurate predictions by machine learning models. The proposed method was tested using a dataset of 140 DRs and achieved a classification accuracy of 97.4%, with a sensitivity of 80.9% and a specificity of 94.8%. These results demonstrate that the Firefly algorithm-based feature selection significantly outperforms traditional methods in diagnosing IANI. The novelty of this research lies in its integration of advanced feature selection techniques with support vector machines, offering a robust tool for improving diagnostic accuracy in dental imaging. This work contributes to enhanced clinical decision-making and could be valuable for broader applications in healthcare systems.

Keywords: Digital Radiographs, Feature Selection, Firefly, Health System, Inferior Alveolar Nerve Injury, Support Vector Machine

1. Introduction

Medical needs have fueled the rapid development of medical image processing techniques, which has significantly raised the bar for therapeutic outcomes. They are now necessary instruments for diagnosis, therapy planning, and treatment administration verification. Thus, medical image processing technology has long caught the interest of pertinent specialists. Currently, panoramic radiography is a common tool in dentistry because it makes anatomical structures in pathological changes to the jaws, temporomandibular joints, and teeth visible. An artificial root called a dental implant is surgically put into the mandible to serve as a platform for a dental prosthesis. Major medico-legal ramifications stem from IANI, which is the primary problematic importance of dental surgical treatments [1]. These lesions to the buccal oral mucosa, lower teeth, and ipsilateral skin of the lower lip and cheek cause partial or total loss of consciousness. IANI can be brought on by the implantation of dental implants, local anesthetic injections, surgery on the third molar, endodontic treatment, trauma, and orthognathic surgery.

IANI and lingual nerve (LN) injuries are influenced by many anatomical, treatment-related, and demographic parameters, and are thought to be amenable to mechanical irritations from surgical interference [2]. Depending on the extent of the nerve injury, the majority of patients who receive an IANI progressively return to normal consciousness over the course of a few weeks or months. However, revival will be incomplete following the most severe injuries, where there is a fraction/fracture or whole sectioning of the nerves, and the area may have been contaminated by

***Corresponding author: P. Manikandaprabhu (manipsgphd@gmail.com)**
DOI: https://doi.org/10.47738/jads.v5i3.356

infection. Consequently, while employing preoperative planning software for dental implant surgery, IAN identification is crucial.

The Inferior Alveolar Nerve (IAN) is the core sensory nerve that provides sensory innervations to the lower teeth as well as the lower lip and some skin on the lower face. The IAN passes via a mandibular canal, also known as the inferior alveolar canal (IAC), that runs through the mandible bone. The IAC's radiographic evaluation can be used to determine the IAN's final evaluation because it is located inside it.

The IAC has a hollow tubular shape, but because it is often connected to other empty areas and has an unclear structure, it is challenging to identify. As a result, precisely and automatically identifying the IAN canal is a difficult problem. Encircling the IAC are two slender radiopaque outlines that depict the cortical walls of the canal. IAC is positioned behind or above the mandibular molar teeth's apex [3]. Because of this, most previous research on IAC identification [4] has required user participation, such as a manual IAN canal trace. Extremely dangerous consequences may result from IAN damage [5].

On panoramic Digital Radiography (DR) observation, the root apex of the mandibular second molar was in close propinquity to the mandibular canal while the apices of the mesial and distal roots of the mandibular first molar were the farthest from the canal [6]. Radiological prediction of injury to the IAN depends on the connection between the root and the canal that Malik [7] discussed. Rood and Shebab [8] have defined seven vital recommendations that can be taken from OPG images. There have been several OPG assessment studies that maintain the effectiveness of these seven findings [9]. It must be renowned, even if, that the statistical results from these analyses had various levels of specificity and sensitivity in table 1. Nowadays, research has determined that high-risk signs are known by OPG in particular; darkening of the root is closely related to cortical bone loss and/or grooving of the root [9].

2. Related Work

Image categorization [10] has emerged as a prominent field in computer vision, focusing on the automatic classification of unknown images based on their visual features. This task is critical in numerous applications, including medical imaging, surveillance, and object recognition. The stages following feature extraction, such as feature selection and classification, play an instrumental role in influencing the overall performance and accuracy of the image categorization process. Key visual attributes such as color, shape, and texture are often regarded as fundamental components in feature extraction. However, the analysis of medical images, especially X-ray images, presents unique challenges since these images are typically grayscale, lacking any color information. As a result, texture-based feature extraction methods have gained significant traction among researchers [11], [12], [13], [14], as they provide a robust means of extracting meaningful patterns from grayscale images.

For instance, Mueen et al. [15] introduced a comprehensive approach that combines multiple visual features to improve classification performance. Their methodology incorporates the Gray Level Co-occurrence Matrix (GLCM) for texture analysis, a shape-based Canny edge detector for detecting image contours, and pixel values as a global image descriptor. This amalgamation of features proved effective in creating a more descriptive and richer feature vector, which is crucial for complex image classification tasks. Several other studies have also explored the use of pixel values, integrated with various image representation techniques, to enhance feature extraction. These efforts [16] have shown that combining pixel values with other features can improve the overall representation of images, especially in cases where texture and shape features alone may not be sufficient.

In the domain of medical image analysis, texture analysis plays a pivotal role, particularly in the diagnosis of diseases through imaging techniques. Numerous studies have highlighted the importance of texture-based feature extraction techniques, with GLCM being one of the most widely used methods. GLCM has been employed in a range of applications, from lung nodule detection to breast cancer prognosis. For example, Yu et al. [11] utilized GLCM histograms to extract features from Digital Radiograph (DR) images, which were then used to construct a feature vector for classification. Katsuragawa et al. [12] introduced a geometric pattern feature analysis approach based on texture to analyze DR images. Their method successfully identified subtle patterns in the texture of the images, contributing to more accurate diagnostic decisions.

Moreover, several advanced classification techniques have been proposed to further refine the use of texture-based features. The PCADT classification method presented in [13] integrated GLCM with embedded zero tree wavelet features to enhance classification accuracy in medical image analysis. Similarly, the authors of [14] proposed a PCA-MLP classification approach, leveraging both GLCM and embedded zero tree wavelet features for improved classification of X-ray images. This technique demonstrated superior performance by reducing the dimensionality of the feature space while preserving the most critical information needed for accurate classification.

Building on these efforts, Mueen et al. [15] introduced a unified classification model that combines Random Forest (RF) and Support Vector Machine (SVM) techniques. This model utilizes embedded zero tree wavelet and GLCM features for feature extraction, while the Firefly (FF) algorithm is employed for feature selection [16]. The integration of RF and SVM in this unified model allows for better handling of the high-dimensional feature space, improving the classification accuracy by effectively managing overfitting and enhancing generalization.

SVM have gained widespread acceptance as a powerful tool for binary classification tasks. SVM has been employed extensively in medical image classification due to its robustness in handling high-dimensional data and its ability to create decision boundaries that maximize the margin between classes. Zhu et al. [17] utilized an SVM with a Gaussian kernel classifier to distinguish between benign and malignant pulmonary nodules in lung images. Their approach demonstrated superior performance in accurately classifying nodules, further validating the effectiveness of SVM in medical image analysis.

Additionally, Yuan et al. [18] applied SVM to breast cancer prognosis classification, showing that the SVM model outperforms other classifiers in terms of accuracy and predictive power. This was particularly evident in their ability to differentiate between various stages of cancer progression, highlighting the versatility and effectiveness of SVM in handling complex medical image datasets. Moreover, SVM has been used beyond traditional medical image classification tasks. For example, SVM models have been employed to automatically detect medical-related messages [19], proving their effectiveness in a variety of health-related applications.

Given the strong performance of SVM in previous studies, this research adopts SVM as the primary classification tool. The choice of SVM is based on its proven ability to handle binary classification problems efficiently, especially in medical image analysis, where precise classification can have significant implications for diagnosis and treatment. This study builds on the work of previous researchers by leveraging SVM in combination with advanced feature extraction and selection techniques to enhance the accuracy of image categorization in a medical context.

3. Proposed Methodology

Figure 1 illustrates the proposed methodology framework, which is structured into four key stages: pre-processing, feature extraction, feature selection, and classification. In the pre-processing stage, raw data is cleaned and transformed to ensure consistency and readiness for further analysis. Following this, the feature extraction phase focuses on identifying and extracting key attributes from the dataset, reducing its complexity while preserving essential information. The feature selection step then aims to isolate the most relevant features by eliminating redundant or irrelevant data, optimizing the model's performance. Finally, the classification stage employs machine learning algorithms to categorize the data based on the selected features. This structured approach enhances the accuracy and efficiency of the overall analysis.

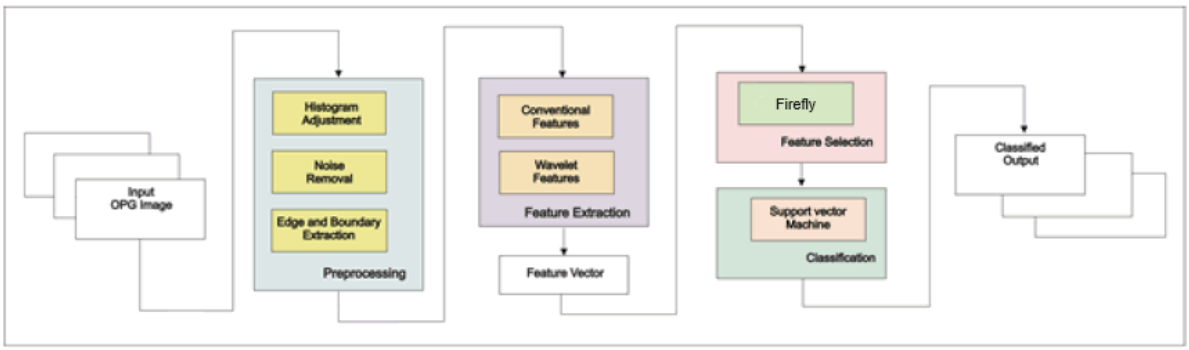

Figure 1. Proposed Methodology Framework

3.1. Preprocessing

Pre-processing consists of normalizing the intensity variations, low contrast, removing low-frequency noise, removing reflections, and masking segments of images. This stage is crucial to the accurate and flawless extraction of features. Sublevels of this technique include canny-based edge extraction, noise reduction, and histogram modification.

Histogram adjustment: It justifies the gray-level histogram of input photos by emphasizing and highlighting their details [20]. In this instance, mapping the input intensity picture values to new values increases the contrast of all the images by ensuring that 1% of the data is saturated at both low and high input data intensities shown in figure 2.

Figure 2. OPG image before preprocessing

Noise Removal: The anisotropic diffusion filter described in [20] is used to remove noise and extraneous information. This filter eliminates noise from the input image while maintaining key components, like edges and major boundaries. The anisotropic diffusion equation's solution is used to model the filtered image as follows: as the solution to the anisotropic diffusion equation as follows:

$$\frac{\partial \mathrm{u}(\mathrm{x},\mathrm{y},\mathrm{t})}{\partial \mathrm{t}} = \mathrm{div}(\mathrm{g}(|\nabla \mathrm{u}(\mathrm{x},\mathrm{y},\mathrm{t})|)\nabla \mathrm{u}(\mathrm{x},\mathrm{y},\mathrm{t})) \quad (1)$$

Note: $u(x,y,t):\Omega \times [0,+\infty] \to R$ is a scale image and $g(|\nabla u|)$ is a decreasing function depending on the gradient of u.

Edge and Boundary extraction: An edge provides an object's layout. Finding the value of each pixel and comparing it to the surrounding pixels to define edge regions [21]. When the intensities are precisely measured, every object in the image is delineated [22]. Clever edge detection techniques [21] are used to extract boundaries and edges from photos. Figure 3 illustrates the Canny edge detection process for segmentation.

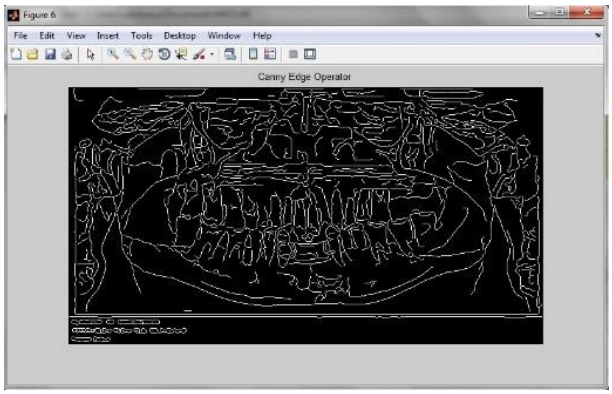

Figure 3. OPG image for After Edge and Boundary Detection

3.2. Feature Extraction

Generally, low-level elements like color, shape, and texture are used for image classification. That being said, most DR photos are grayscale. For DR analysis, color is therefore an inappropriate characteristic. DR analysis can then take

 ISSN 2723-6471

shape and texture into account [12]. The traditional traits in figure 4 were extracted in this manner: Shape, region attributes, Tamura features, entropy, and wavelet-based texture features are looked at in θ directions (θ =0°, 45°, 90°, 135°). This is for a two-dimensional discrete wavelet transform with four sub-bands (LL, LH, HL, and HH). 383 features were taken out of each DR image in this instance.

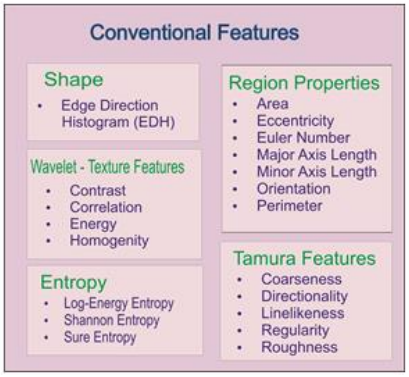

Figure 4. Conventional features

Shape features: An object's shape in an image conveys geometric information about it. Even when the object's orientation, scale, and location are altered, this geometrical information stays the same. In this study, an image's edges are used to express its shape information. A histogram of the edge directions represents the shape property for each image patch and picture. Edge histograms are produced using the clever edge operator [23].

Wavelet-texture features: The segmented image is used to generate a variety of statistical features for classification [24]. However, extracting a good feature set for classification is a difficult task. The joint probability distribution of pixel matchups serves as the foundation for GLCM features. The joint probability distribution between pixels is computed using the distance and angle ¸ within a specified neighborhood. For computation, d=1, 2 and ¸=0°, 45°, 90°, and 135° are typically employed [25]. Thus, each DR image contained a total of 32 characteristics. To extract the GLCM properties (energy, local fluctuations, correlation, and homogeneity) from our suggested system [26].

Region properties: The perimeter, eccentricity, Euler number, area, major axis length, minor axis length, and picture orientation are the common region properties [27]. The lengths of the minor and major axes of the ellipse that have the same normalized second central moments as the region or an object, respectively, are known as the minor and major axis lengths. The ratio of the smallest to the largest eigenvalue is known as eccentricity. The number of connected components and holes in an item or region is subtracted to get the Euler number. The direction of the greatest eigenvector of an object's or region's second order covariance matrix can be used to describe orientation. The number of pixels on the object boundary is known as the perimeter, while the number of pixels inside the boundary is known as the area.

Tamura features: There are 6 different Tamura features: coarseness, contrast, directionality, line likeness, regularity and roughness [28]. In the literature [29], the first three features are used since they are strongly correlated with human perception.

3.3. Feature Selection

One of the most significant problems in data science and machine learning is feature selection [16]. This procedure is typically carried out at the data preprocessing stage when the data is formatted appropriately for the machine learning algorithm to use in subsequent operations. In data mining and machine learning, feature selection is a pre-processing technique that lowers the dimensionality of data by eliminating noise and superfluous features, with the goal of producing an ideal or nearly ideal feature subset. The technique of selection and the evaluation criteria are two fundamental ideas in feature selection. Three primary feature selection procedures consider assessment criteria: wrapper-based, filter-based, and embedding methods.

Utilizing statistical measures to assign scores to each feature, filter-based approaches like Gini Index, Information Gain, Relief, FOCUS, and Chi-Square [30] rank features and select a subset based on the scores. The wrapper-based approach chooses the best attribute subset by applying machine learning algorithms. Wrapper-based approaches are

most frequently used in feature selection procedures due to their improved classification accuracy, despite their greater processing costs. The wrapper-based and filter-based techniques are utilized by the embedded methods since they are combined with them. The most promising approaches to feature selection are metaheuristics, particularly those inspired by nature, such as swarm intelligence and evolutionary algorithms (EA), because of the vast search area. Metaheuristics are frequently applied as cover techniques for problems involving feature selection. For instance, the genetic algorithm (GA) [31] demonstrated a successful wrapper-based technique for this task.

Swarm intelligence is a very effective and reliable optimizer for a wide range of real-world NP-hard problems from different areas, such as COVID-19 case predictions and wireless sensor networks. By carrying out exploration and exploitation procedures, these techniques mimic natural systems. The fundamental concept underlying this class of algorithms is the incorporation of naturally guided random search techniques into the optimization process. Ant colony optimization, artificial bee colonies (ABC), bat algorithms (BA), particle swarm optimization (PSO) [32], and the FA [16] are a few of the most well-known applications of swarm intelligence. A variety of swarm intelligence techniques have been used recently for feature selection. Here, the Firefly algorithm [16] is used as a Feature Selection method.

Firefly Algorithm: The Firefly Algorithm (FF) is an optimization algorithm that draws inspiration from nature and falls under the larger category of swarm intelligence algorithms [16]. It takes its cues from the way fireflies in the wild flash, utilizing bioluminescence as a means of courtship and communication. The Firefly Algorithm, created by Xin-She Yang in 2008 [33], has grown in favor of a reliable and adaptable optimization method for handling challenging optimization issues.

To realize that FF (18) is implemented shown in figure 5. It's an innovative program that was motivated by Firefly' social interactions. The majority of the two thousand or so species of fireflies generate brief, rhythmic flashes that serve as a way of communication amongst them. To draw in more fireflies is, thus, the purpose of a firefly's flash. FA was proposed, which follows these three rules, by idealizing parts of the firefly's flashing characteristics: The degree of a firefly's attraction is directly related to its brightness; all fireflies, regardless of gender, are attracted to one another. More brightness equals a shorter distance between two fireflies, so for any two flashing fireflies, the less bright one will travel towards the brighter one. An evaluation of the fitness function establishes a firefly's brightness. One possible relationship between the brightness and the value of the objective function (fitness function) in a maximization issue is this.

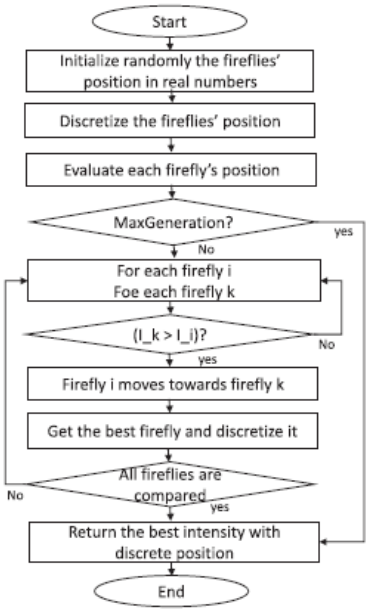

Figure 5. Flowchart of Firefly Algorithms

Table 1 provides an overview of the sensitivity values for predicting IAN injury associated with the third molar using Orthopantomogram (OPG) imaging. Sensitivity, which indicates the ability of the imaging procedure to correctly

 ISSN 2723-6471

identify cases of IAN injury, is presented for three key radiographic features: darkening of the root, interruption of the canal, and diversion of the canal.

Table 1. Specificity and Sensitivity for Predicting Ian Injury with the Third Molar

OPG Imaging procedure	Sensitivity (%)
Darkening of the root	32-71
Interruption of the canal	22-80
Diversion of the canal	3-50

The sensitivity of the darkening of the root ranges from 32% to 71%, suggesting moderate reliability in identifying IAN injury. This variability reflects that in certain cases, this feature serves as a stronger predictor, while in others, its predictive power is reduced. Similarly, the sensitivity for interruption of the canal fluctuates widely, between 22% and 80%, indicating that it can be an effective predictor in some instances but less reliable in others. In contrast, the sensitivity for diversion of the canal is notably lower, ranging from 3% to 50%, making it a weaker predictor overall, though it may offer moderate predictive value in certain cases.

3.4. Classification

Vapnik [35] presented the SVM in the middle of the 1990s. It functions well in high-dimensional areas and with small sample sizes [17]. Additionally, it takes advantage of the least practical quadratic programming problems, which are quickly and methodically identified. Both computing time and scaling are much improved. Using linear kernels, it carries out the lowest sequential maximization process to train a classifier.

One of the key advancements in machine learning algorithms is the kernel-based SVM approach. SVM is a collection of supervised learning techniques that are useful for regression and classification. It picks up item labeling skills by observation. SVM has demonstrated its abilities in pattern identification and outperforms other machine learning algorithms in a variety of domains. Additionally, SVMs are being successfully used in a growing range of biological applications. SVM has demonstrated a superior generalization performance compared with other classification algorithms, based on empirical results and several classification applications in the automatic categorization of medical X-ray pictures [36], [37].

There are two divisions in our suggested system's classification: the training stage and the testing stage. Different features are taken from the IAN-identified and unidentified photos during the training phase. The classifier divides the image into IAN-identified and not-identified images during the testing step based on the knowledge base. The proposed FF-SVM model for the feature selection-based classification model is displayed in figure 6.

Step-1: Initialize all data into an entire dataset.
Step-2: Use Firefly algorithm to rank the features.
Step-3: Evaluate aggregate voting to the ranked features.
Step-4: Update working dataset by removing less important features. Until the number of features are small.
Step-5: Apply SVM with RBF Kernel into the reduced features.

$$\min\left(\frac{1}{2}\|w\|^2 + c\sum_{i=1}^{m}\xi_i\right) \quad \text{(a)}$$

subject to:

$$y_i(w^T x_i + b) \geq 1 - \xi_i, \quad \xi_i \geq 0, \quad i = 1,\mathrm{K}\,,m \quad \text{(b)}$$

where w is a weight vector and b is bias. The variables ξ_i are positive slack variables, which is necessary to allow misclassification.

Step-6: Consider parameter C seeks to penalize decision error when searching for the maximum marginal hyperplane.

$$y = f(x) = \mathrm{sgn}(w^T \phi(x) + b) \quad \text{(c)}$$

where Φ is the mapping function and x is a training sample.

Step-7: Choose the best parameter for create as a Classification Model.

Figure 6. Proposed Model for FF-SVM

4. Experimental Results and Discussions

4.1. Dataset Description

In this instance, 140 OPG DRs were gathered from the Saranya Dental Clinic in Somanur, Coimbatore. Of these, 62 OPG radiographs were taken of male patients aged 10 to 75 and 38 of female patients aged 12 to 74. For precise implant positioning and identification of IAN injuries, about 40 posterior dental implants are included in OPG radiographs. A panel of radiologists made the diagnoses for each of the 100 cases. The OPG image summary from table 2 and the patient data summary with age range and sex from table 3 are displayed.

Table 2. Summary of Experimental Data

Patient Age (Years)	Sex	Number of Patients	Number of DRs	Data Dimensions
10-75	Male-62 Female-38	100	140	1024 × 564 ×24

Table 3 summarizes the patient data based on sex and age range, illustrating the distribution of male and female patients across various age groups. In the 10 to 20 age range, there are 15 male and 8 female patients, totaling 23. The largest group falls within the 21 to 35 age range, with 27 male and 20 female patients, contributing to a total of 47. In the 36 to 50 age range, there are 22 male and 17 female patients, amounting to 39. For the 51 to 65 age group, 10 male and 8 female patients are recorded, making up 18 in total. The oldest group, aged 66 to 75, includes 9 male and 4 female patients, totaling 13. Overall, the dataset comprises 140 patients, with a higher proportion of males (83) compared to females (57) across all age ranges, particularly in the 21 to 35 and 36 to 50 age groups.

Table 3. Patients Data Summary with Sex and Age Range

Age	Male	Female	Total
10 to 20	15	8	23
21 to 35	27	20	47
36 to 50	22	17	39
51 to 65	10	8	18
66 to 75	9	4	13
Total	83	57	140

4.2. Performance Assessment

In this study, classification accuracy, sensitivity, and specification were used as assessments of the proposed RFSVM model. It is defined in Equations (2), (3), and (4).

$$\text{Accuracy} = \frac{\text{TP} + \text{TN}}{\text{TP} + \text{FN} + \text{TN} + \text{FP}} \times 100\% \quad (2)$$

$$\text{Sensitivity}=\text{TP}/(\text{TP}+\text{FN})\times 100\% \quad (3)$$

$$\text{Specificity} = \frac{\text{TN}}{\text{TN} + \text{FP}} \times 100\% \quad (4)$$

Where TP (True Positive) denotes the number of correctly classified IAN injured objects, TN (True Negative) denotes the number of correctly classified healthy objects, FP (False Positive) denotes the number of normal cases incorrectly classified. IAN denotes injured objects, and FN (False Negative) denotes the number of irregular objects incorrectly classified as normal objects.

4.3. Comparison of Classification Performance

Table 4 and table 5 present the experimental data that were obtained using the suggested technique. Multilayer Perceptron (MLP) and Decision Tree (DT) classifiers are not as accurate as SVM classifiers. FF - SVM achieves higher classification accuracy of 83.58% and 96.4% in the testing and training phases, respectively. The comparison of the suggested outcomes with the current results is displayed graphically in figure 7 [13], [14], [33], [36].

Table 4 presents a comparison of the training results obtained from various classifiers combined with different feature selection methods, evaluated based on classification accuracy, sensitivity, and specificity. The PCA-DT classifier [13] achieved a classification accuracy of 82.3%, with a sensitivity of 76.2% and a specificity of 85.2%, indicating moderate performance. The PCA-MLP model [14] improved upon this, with a higher accuracy of 85.4%, similar sensitivity of 76.6%, and an enhanced specificity of 90.2%, reflecting a better ability to correctly identify negative cases.

Further improvement is seen with the PSO-MLP model [36], which achieved 88.7% accuracy, a notable increase in sensitivity (85.2%), and balanced specificity (88.5%), making it more effective in identifying positive cases. The RF-SVM classifier [33] significantly advanced performance with 96.4% accuracy, 88.2% sensitivity, and a high specificity of 99.1%, indicating strong discriminatory power between true positive and true negative cases.

The proposed FF-SVM model demonstrated the highest performance across all metrics, achieving 97.4% classification accuracy, 89.2% sensitivity, and 99.1% specificity. These results suggest that the combination of the Firefly (FF) algorithm for feature selection and SVM for classification provides a more robust and accurate model, outperforming the other methods in both identifying true positives and avoiding false positives. This highlights the proposed method's effectiveness in predictive tasks, making it the most reliable approach in this comparison.

Table 4. Comparison of Training Results with Different Classifiers

Feature Selection - Classifier	Classification Accuracy	Sensitivity	Specificity
PCA-DT [13]	82.3	76.2	85.2
PCA-MLP [14]	85.4	76.6	90.2
PSO-MLP [36]	88.7	85.2	88.5
RF-SVM [33]	96.4	88.2	99.1
Proposed FF-SVM	97.4	89.2	99.1

Table 5 presents a comparison of testing results for various classifiers employing different feature selection techniques, focusing on their performance in terms of classification accuracy, sensitivity, and specificity. The PCA-DT classifier [13] achieved a classification accuracy of 78.58%, with a sensitivity of 68.6% and a specificity of 76.8%. This reflects a moderate performance, indicating that while the classifier performs reasonably well, there is room for improvement in correctly identifying both positive and negative cases.

The PCA-MLP model [14] showed slight improvements, with a classification accuracy of 79.29%, 69.9% sensitivity, and 83.8% specificity. This model offers better specificity compared to PCA-DT, suggesting an enhanced ability to correctly identify true negatives, although its sensitivity remains relatively similar. Further advancements were observed with the PSO-MLP classifier [36], which achieved an accuracy of 80.71%, 77.6% sensitivity, and 80.5% specificity. This classifier improves both sensitivity and specificity, demonstrating a more balanced performance in detecting positive cases while minimizing false positives.

The RF-SVM classifier [33] demonstrated a significant increase in performance, with a classification accuracy of 83.58%, 79.9% sensitivity, and 92.8% specificity. This model excels in both identifying true positives and true negatives, indicating its superior effectiveness in classification tasks. The proposed FF-SVM model achieved the highest performance across all metrics, with a classification accuracy of 85.58%, 80.9% sensitivity, and 94.8% specificity. This model outperforms all other classifiers, showcasing its exceptional ability to accurately classify cases, both positive and negative, during testing.

Table 5. Comparison of Testing Results with Different Classifiers

Feature Selection - Classifier	Classification Accuracy	Sensitivity	Specificity
PCA-DT [13]	78.58	68.6	76.8
PCA-MLP [14]	79.29	69.9	83.8
PSO-MLP [36]	80.71	77.6	80.5
RF-SVM [33]	83.58	79.9	92.8
Proposed FF-SVM	85.58	80.9	94.8

 ISSN 2723-6471

Figure 7 illustrates the graphical results of classification accuracy across different models or classifiers evaluated in the study. The figure provides a visual representation of how each classifier performs in terms of classification accuracy, offering a clear comparison of their effectiveness. In the graph, the x-axis typically represents the different classifiers or models assessed, while the y-axis displays the classification accuracy percentage. Each bar or data point in the graph corresponds to the accuracy achieved by a specific classifier, allowing for an immediate visual comparison of their performance.

From the figure, it is evident that some classifiers achieve higher accuracy than others. The graphical results clearly show which models excel in accurately classifying cases and which ones have lower accuracy, providing insights into the relative strengths and weaknesses of each classifier. This visual comparison helps in understanding the performance differences and identifying the most effective model for the classification task at hand.

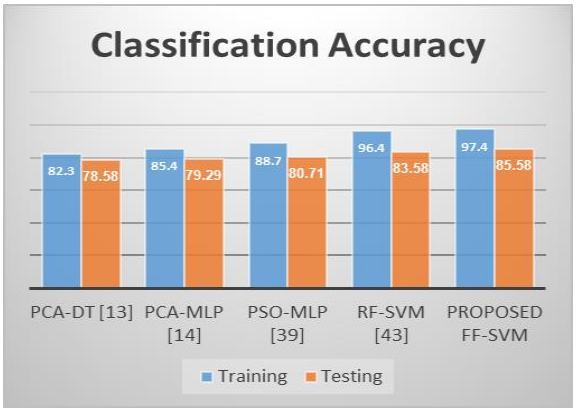

Figure 7. Graphical Results of Classification Accuracy

5. Conclusion

The inferior alveolar nerve, which traverses the lower jaw, is susceptible to damage during dental procedures, potentially resulting in IANI. This condition can arise from factors such as improper anesthetic administration, surgical trauma, or implant placement. Severe cases of IANI may lead to irreversible nerve damage, manifesting as numbness, tingling, or discomfort in the lower lip, chin, and teeth. Accurate classification of IANI is crucial for effective management and treatment, as it assists dentists in selecting the appropriate intervention and assessing the extent of the injury. The Seddon classification is the predominant system for categorizing IANI, which includes three types: neuropraxia, axonotmesis, and neurotmesis. Digital radiography is essential for this classification, as it provides detailed images of the affected area, enabling informed decision-making.

This research presents a novel approach that combines texture and shape feature extraction using the EZW-based FF-SVM model. Applied to a dataset of 140 digital radiographs (DRs), our method involved extracting various conventional features to enhance classification accuracy. The feature selection and classification were performed using the Firefly-based Support Vector Machine model. The experimental results show that our approach achieved a classification accuracy of 85.58%, a sensitivity of 80.9%, and a specificity of 94.8%. These results indicate that our proposed method outperforms other approaches in terms of classification accuracy. The superior performance in sensitivity and specificity highlights the effectiveness of our model in accurately identifying IANI. Overall, the findings demonstrate the robustness of our proposed FF-SVM model, providing a reliable tool for improving the precision of IANI classification.

6. Declarations

6.1. Author Contributions

Conceptualization: P.M., C.T., M.B., and Z.X.; Methodology: C.T.; Software: P.M.; Validation: P.M. and C.T.; Formal Analysis: P.M. and C.T.; Investigation: P.M.; Resources: C.T.; Data Curation: C.T.; Writing Original Draft Preparation: P.M., C.T., and M.B.; Writing Review and Editing: C.T. and P.M.; Visualization: P.M.; All authors have read and agreed to the published version of the manuscript.

6.2. Data Availability Statement

The data presented in this study are available on request from the corresponding author.

6.3. Funding

The authors received no financial support for the research, authorship, and/or publication of this article.

6.4. Institutional Review Board Statement

Not applicable.

6.5. Informed Consent Statement

Not applicable.

6.6. Declaration of Competing Interest

The authors declare that they have no known competing financial interests or personal relationships that could have appeared to influence the work reported in this paper.

References

[1] R. A. Mischkowski, M. J. Zinser, J. Neugebauer, A. C. Kübler, and J. E. Zöller, "Comparison of static and dynamic computer-assisted guidance methods in implantology," *International Journal of Computerized Dentistry*, vol. 9, no. 1, pp. 23–35, Jan. 2006.

[2] J. Mansoor, "Pre-and postoperative management techniques. Before and after. Part 2: the removal of third molars," *British Dental Journal*, vol. 218, no. 5, pp. 279-284, 2015.

[3] C. K. Modi and N. P. Desai, "A simple and novel algorithm for automatic selection of roi for Dental Radiograph segmentation," *2011 24th Canadian Conference on Electrical and Computer Engineering(CCECE)*, vol. 5, no. May, pp. 000504–000507, May 2011. doi:10.1109/ccece.2011.6030501

[4] N. E. O'Murchu, "Dental radiography: principles and techniques, 4th edition," *British Dental Journal*, vol. 211, no. 9, pp. 440–440, Nov. 2011.doi: 10.1038/sj.bdj.2011.957

[5] S.C.White, and M.J.Pharoah, "Oral radiology-E-Book: Principles and interpretation", Elsevier Health Sciences, 2014.

[6] I. Sato, R. Ueno, T. Kawai, and Takashi Yosue, "Rare Courses of the Mandibular Canal in the Molar Regions of the Human Mandible: A Cadaveric Study," *Okajimas Folia Anatomica Japonica*, vol. 82, no. 3, pp. 95–102, Jan. 2005. Doi: 10.2535/ofaj.82.95

[7] T. Wahyuningsih and D. Sugianto, "Temporal Patterns in User Conversions: Investigating the Impact of Ad Scheduling in Digital Marketing," *J. Digit. Mark. Digit. Curr.*, vol. 1, no. 2, pp. 165-182, 2024.

[8] Hang Gul Kim and Jae Hoon Lee, "Analysis and evaluation of relative positions of mandibular third molar and mandibular canal impacts*," Journal of The Korean Association of Oral and Maxillofacial Surgeons,* vol. 40, no. 6, pp. 278–278, Jan. 2014.

[9] J.-W. Kim, I.-H. Cha, S.-J. Kim, and M.-R. Kim, "Which Risk Factors Are Associated With Neurosensory Deficits of Inferior Alveolar Nerve After Mandibular Third Molar Extraction?," *Journal of Oral and Maxillofacial Surgery*, vol. 70, no. 11, pp. 2508–2514, Nov. 2012.

[10] T. Karthikeyan and P. Manikandaprabhu, "Analyzing urban area land coverage using image classification algorithms," *in Computational Intelligence in Data Mining-Volume 2: Proceedings of the International Conference on CIDM, 20-21 December 2014, Springer India*, vol. 2015, no. Dec., pp. 439-447.

[11] P. Yu, H. Xu, Y. Zhu, C. Yang, X. Sun, and J. Zhao, "An Automatic Computer-Aided Detection Scheme for Pneumoconiosis on Digital Chest Radiographs," *Journal of Digital Imaging*, vol. 24, no. 3, pp. 382–393, Feb. 2010.

[12] S Katsuragawa, K. Doi, H. MacMahon, L Monnier-Cholley, J. Morishita, and T. Ishida, "Quantitative analysis of geometric-pattern features of interstitial infiltrates in digital chest radiographs: Preliminary results*," Journal of Digital Imaging,* vol. 9, no. 3, pp. 137–144, Aug. 1996.

[13] T. Karthikeyan and P. Manikandaprabhu, "A Novel Approach for Inferior Alveolar Nerve (IAN) Injury Identification using

Panoramic Radiographic Image," *Biomedical and Pharmacology Journal*, vol. 8, no. 1, pp. 307–314, Jun. 2015.

[14] T.Karthikeyan, P.Manikandaprabhu, "A Study on Digital Radiographic Image Classification for Inferior Alveolar Nerve Injury (IAN) Identification using Embedded Zero Tree Wavelet*", Int. Jour. Appl. Engg. Res.*, vol. 10, no. 55, pp. 599-604, June 2015.

[15] Devrim Ünay, Octavian Soldea, Süreyya Özögür-Akyüz, Müjdat Çetin, and Aytül Erçil, "Medical Image Retrieval and Automatic Annotation: VPA-SABANCI at ImageCLEF 2009," CLEF (Working Notes), Sep. 2009.

[16] I. Fister, I. Fister, X.-S. Yang, and J. Brest, "A comprehensive review of firefly algorithms," *Swarm and Evolutionary Computation*, vol. 13, no. 1, pp. 34–46, Dec. 2013.

[17] Y. Zhu, Y. Tan, Y. Hua, M. Wang, G. Zhang, and J. Zhang, "Feature Selection and Performance Evaluation of Support Vector Machine (SVM)-Based Classifier for Differentiating Benign and Malignant Pulmonary Nodules by Computed Tomography," *Journal of Digital Imaging*, vol. 23, no. 1, pp. 51–65, Feb. 2009.

[18] B. Zheng, S. W. Yoon, and S. S. Lam, "Breast cancer diagnosis based on feature extraction using a hybrid of K-means and support vector machine algorithms," *Expert Systems with Applications*, vol. 41, no. 4, Part 1, pp. 1476–1482, Mar. 2014.

[19] Y. Lu, "Automatic topic identification of health-related messages in online health community using text classification," *SpringerPlus*, vol. 2, no. 1, pp. 1-12, Jul. 2013.

[20] F. Cervantes-Sanchez, I. Cruz-Aceves, A. Hernandez-Aguirre, M. A. Hernandez-Gonzalez, and S. E. Solorio-Meza, "Automatic Segmentation of Coronary Arteries in X-ray Angiograms using Multiscale Analysis and Artificial Neural Networks," *Applied Sciences*, vol. 9, no. 24, pp. 5507-5514, Jan. 2019.

[21] S. Fu, Q. Ruan, W. Wang, and Y. Li, "Adaptive Anisotropic Diffusion for Ultrasonic Image Denoising and Edge Enhancement," *Zenodo (CERN European Organization for Nuclear Research)*, vol. 23, no. No., pp. 975-978, Nov. 2008.

[22] J. Canny, "A Computational Approach to Edge Detection," *IEEE Transactions on Pattern Analysis and Machine Intelligence*, vol. PAMI-8, no. 6, pp. 679–698, Nov. 1986.

[23] Feng Pan et al., "Fast mode decision algorithm for intraprediction in H.264/AVC video coding," *in IEEE Transactions on Circuits and Systems for Video Technology*, vol. 15, no. 7, pp. 813-822, July 2005.

[24] R. M. Haralick, K. Shanmugam, and I. Dinstein, "Textural Features for Image Classification*," IEEE Transactions on Systems, Man, and Cybernetics*, vol. SMC-3, no. 6, pp. 610–621, Nov. 1973.

[25] A. Gelzinis, A. Verikas, and M. Bacauskiene, "Increasing the discrimination power of the co-occurrence matrix-based features," *Pattern Recognition*, vol. 40, no. 9, pp. 2367–2372, Sep. 2007.

[26] Subramoniam, Barani, and Rajini, "A non-invasive computer aided diagnosis of osteoarthritis from digitalx-ray images," *Biomedical Research-tokyo*, vol. 26, no. 4, p. 1-7, Jan. 2015.

[27] None Po-Cheng Wu and None Liang-Gee Chen, "An efficient architecture for two-dimensional discrete wavelet transform," *IEEE Transactions on Circuits and Systems for Video Technology*, vol. 11, no. 4, pp. 536–545, Apr. 2001.

[28] K. Masood and N. M. Rajpoot, "Spatial Analysis for Colon Biopsy Classification from Hyperspectral Imagery," Jan. 2008.

[29] Z. Li, X. Zhang, H. Müller, and S. Zhang, "Large-scale retrieval for medical image analytics: A comprehensive review," *Medical Image Analysis*, vol. 43, no. 1, pp. 66-84, 2018.

[30] Berlilana and A. Mu'amar, "Economic Decentralization through Blockchain Opportunities Challenges and New Business Models", *J. Curr. Res. Blockchain.*, vol. 1, no. 2, pp. 112–123, Sep. 2024.

[31] G. Chandrashekar and F. Sahin, "A survey on feature selection methods," *Computers and Electrical Engineering*, vol. 40, no. 1, pp. 16–28, Jan. 2014.

[32] D. Sugianto and A. R. Hananto, "Geospatial Analysis of Virtual Property Prices Distributions and Clustering," *Int. J. Res. Metav.*, vol. 1, no. 2, pp. 127-141, 2024.

[33] Manik, aprabhu P, and Karthikeyan T, "Unified RF-SVM model based digital radiography classification for Inferior Alveolar Nerve Injury (IANI) identification.," *Biomedical Research-tokyo*, vol. 27, no. 4, pp. 1107–1117, Jan. 2016.

[34] K. Fawagreh, M. M. Gaber, and E. Elyan, "Random forests: from early developments to recent advancements," *Systems Science & Control Engineering*, vol. 2, no. 1, pp. 602–609, Oct. 2014.

[35] O. Chapelle, P. Haffner, and V. N. Vapnik, "Support vector machines for histogram-based image classification," *IEEE Transactions on Neural Networks*, vol. 10, no. 5, pp. 1055–1064, 1999.

[36] W. Du, Z. Cao, T. Song, Y. Li, and Y. Liang, "A feature selection method based on multiple kernel learning with expression profiles of different types," *BioData Mining*, vol. 10, no. 1, pp. 1-12, Feb. 2017.

[37] N. Gharaei, Z. H. Abdullah, W. Ismail, C. Grosan, and R. Hendradi, "Exercise game rehabilitation of post-injury patients on range of motion: Optimization using genetic algorithms," *AIP Conference Proceedings*, vol. 2562, no. 1, pp. 020002–020010, 2023. doi:10.1063/5.0111469.